Electric quadrupole contribution to resonant x-ray scattering: Application to multipole ordering phases in $Ce_{1-x}La_xB_6$

Tatsuya Nagao
Faculty of Engineering, Gunma University, Kiryu, Gunma 376-8515, Japan

Jun-ichi Igarashi
Faculty of Science, Ibaraki University, Mito, Ibaraki 310-8512, Japan

(Received 10 May 2006; revised manuscript received 20 July 2006; published 5 September 2006)

We study the electric quadrupole ($E2$) contribution to resonant x-ray scattering (RXS). Under the assumption that the rotational invariance is preserved in the Hamiltonian describing the intermediate state of scattering, we derive a useful expression for the RXS amplitude. One of the advantages the derived expression possesses is the full information of the energy dependence, lacking in all the previous studies using the fast collision approximation. The expression is also helpful to classify the spectra into multipole order parameters which are brought about. The expression is suitable to investigate the RXS spectra in the localized f electron systems. We demonstrate the usefulness of the formula by calculating the RXS spectra at the Ce $L_{2,3}$ edges in $Ce_{1-x}La_xB_6$ on the basis of the formula. We obtain the spectra as a function of energy in agreement with the experiment of $Ce_{0.7}La_{0.3}B_6$. Analyzing the azimuthal angle dependence, we find the sixfold symmetry in the σ-σ' channel and the threefold one in the σ-π' channel not only in the antiferro-octupole (AFO) ordering phase but also in the antiferroquadrupole (AFQ) ordering phase, which behavior depends strongly on the domain distribution. The sixfold symmetry in the AFQ phase arises from the simultaneously induced hexadecapole order. Although the AFO order is plausible for phase IV in $Ce_{1-x}La_xB_6$, the possibility of the AFQ order may not be ruled out on the basis of azimuthal angle dependence alone.

DOI: 10.1103/PhysRevB.74.104404 PACS number(s): 75.10.−b, 78.70.Ck, 75.25.+z, 78.20.Bh

I. INTRODUCTION

Resonant x-ray scattering (RXS) has recently attracted much attention, since strong x-ray intensities have become available from the synchrotron radiation. It is described by a second-order process that a core electron is excited into unoccupied states by absorbing incident x rays and that electron is recombined with the core hole by emitting x rays. RXS has been recognized as a useful probe to investigate spatially varying multipole orderings, which the conventional neutron scattering is usually difficult to detect.

For probing the spatial variation of order parameters, x-ray wavelengths need to be order of the variation period. In transition metals, the K edges in the dipole ($E1$) transition are just fitting for this purpose. Actually, by using the K edge, the possibility of the orbital ordering has already been explored in transition-metal compounds.[1,2] The RXS intensities are observed at superlattice Bragg spots, which are interpreted as originating from the modulation in the $4p$ band, since the process involves the excitation of a $1s$ electron to unoccupied $4p$ states.

Because the ordering pattern is usually controlled by electrons in the $3d$ band, the mechanism which causes the modulation is not necessarily trivial. Actually, for most transition-metal compounds, both experimental studies and theoretical studies based on electronic structure calculations have revealed that the RXS intensities are brought about by the hybridization between the $4p$ band and the $2p$ band of the neighboring anions rather than the direct Coulomb interaction between the electron in the $4p$ band and electrons in the $3d$ band.[3,4] This result is reasonable because of the extended nature of the $4p$ state.

On rare-earth metal compounds such as CeB_6, DyB_2C_2, the $L_{2,3}$ edges in the $E1$ transition are used because of the requirement for x-ray wavelength.[5–8] The RXS spectra in the $E1$ transition from the antiferroquadrupole (AFQ) phase of CeB_6 were studied both experimentally[5] and theoretically.[9,10] Although the experiments and the theory give sufficiently consistent results, the relation to the multipole orderings which $4f$ electrons mainly involve is rather indirect, since the resonance is caused by the excitation of a $2p$ electron to $5d$ states. This shortcoming may be overcome by using the quadrupole ($E2$) transition at the $L_{2,3}$ edges, where a $2p$ electron is promoted to partially filled $4f$ states. Using the $E2$ transition has another merit that octupole and hexadecapole orderings are directly detectable. This contrasts with the $E1$ transition, where only dipole and quadrupole orderings are detectable. Of course, intensities in the $E2$ transition are usually much smaller than those in the $E1$ transition.

In this paper, we derive a general formula of the RXS amplitudes in the localized electron picture, in which the electronic structure at each atom is assumed to be well described by an atomic wave function under the crystal electric field (CEF). Historically, the research in such a direction was started by using the framework borrowed from resonant γ-ray scattering.[11] Following the works by de Bergevin and Brunel,[12] Lovesey,[13] and Blume and Gibbs[14] to summarize the nonresonant cross section, Hannon *et al.* have started the investigation on the scattering amplitude of RXS.[15] Since then, several theoretical treatments have been developed.[16–19] The RXS amplitude can be summarized into an elegant form by using vector spherical harmonics. Unfortunately, it has little practical usage because it is difficult to deduce meaningful information when there is no restriction

on the intermediate state of the scattering process. A widely adopted approximation for practical use is the so-called "fast collision approximation" (FCA). This replaces the intermediate state energy in the energy denominator of the RXS amplitude by an averaged value, allowing the denominator out of the summation.[15–19] Thereby, the multiplet splitting of the intermediate state is neglected, leading to an assumed form (usually a Lorentzian form) for the energy profile.

However, recent experiments show deviation from the Lorentzian form in several materials.[20,21] We improve the situation by taking the energy dependence of the intermediate state under the assumption that the intermediate Hamiltonian describing the scattering process preserves spherical symmetry. This assumption is justified when the CEF energy and the intersite interaction are much smaller than the multiplet energy in the intermediate state as is expected in many localized electron materials. We have already reported the formula for the $E1$ transition, having successfully applied to the analysis of the $E1$ RXS spectra in URu_2Si_2 and NpO_2.[22–24] This paper is an extension of those works to the $E2$ transition. The obtained formula makes it possible to analyze the energy profiles of the spectra in contrast with the FCA. In addition, the formula is suitable to discuss the relation of the RXS spectra to multipole order parameters,[20,21,25–28] because it is expressed by means of the expectation values of the multipole order parameters.

We demonstrate the usefulness of the formula by calculating the RXS spectra in multipole ordering phases of $Ce_{1-x}La_xB_6$. Both $Ce_{1-x}La_xB_6$ and its nondiluted material CeB_6 are known to crystallize in the cubic CsCl-type structure ($Pm\bar{3}m$) with the lattice constant $a=4.14$ Å.[29] First, we investigate the $E2$ RXS spectra at the Ce $L_{2,3}$ edges from the AFQ ordering phase (phase II) in CeB_6. Analysis utilizing our formula reveals that the $E2$ RXS spectra in phase II consist of a mixture of the quadrupole and hexadecapole energy profiles. The calculated intensities suggest the possibility that the $E2$ signal at the Ce $L_{2,3}$ edges can be detectable in this material. Note that the ratio of the peak intensities of the spectra at the L_2 and L_3 edges is about a factor 2 smaller than that by the FCA.[30] The reason for such differences is that the FCA is hard to treat properly the interference effect between the energy profiles of rank 2 and rank 4.

For the intermediate doping range $x\approx 0.3-0.5$, $Ce_{1-x}La_xB_6$ falls into a new phase (phase IV) whose primary order parameter is not well established yet.[31] Recently, the $E2$ RXS signals at the Ce L_2 edge have been detected for an $x=0.3$ sample.[27] From the azimuthal angle (ψ) dependence of the peak intensity, it was claimed that the antiferro-octupole (AFO) ordering phase is the most probable candidate because the symmetry of the ψ dependence, sixfold and threefold in the σ-σ' and σ-π' channels, respectively, is deduced from the theory in good agreement with the experiment.[27,32] However, the relative intensity between two channels depends strongly on the domain distribution, and deviates about a factor 2 from the experimental one if the contribution from four domains are added with equal weight. The origin of this discrepancy is still unanswered. It will be pointed out that the RXS peak intensity from the AFQ phase concomitant with the induced hexadecapole contribution also gives rise to the same symmetry of the ψ dependence as obtained from the AFO phase. Thus although the AFO order is plausible in many respects, it seems difficult to rule out the AFQ order on the basis of the azimuthal angle dependence alone. In addition, we calculate the energy dependence of the RXS spectra at the Ce $L_{2,3}$ edges. Assuming both the AFO and AFQ orders, we obtain the spectral shapes at the L_2 edge, which agree with the experimental one for $Ce_{0.7}La_{0.3}B_6$.[27] On the other hand, the spectral shapes at the L_3 edge are found slightly different between two phases, with intensities the same order of magnitude of the reported one at the L_2 edge.

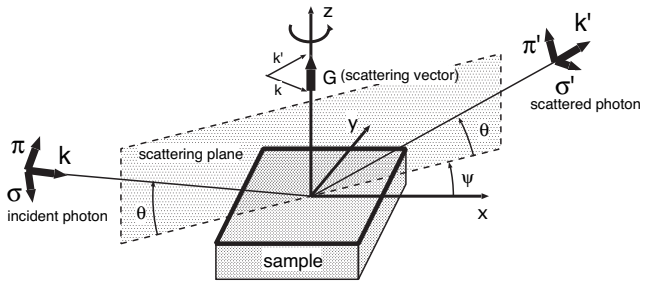

FIG. 1. Geometry of the RXS experiment. Photon with polarization σ or π is scattered into the state of polarization σ' or π' at the Bragg angle θ. The azimuthal angle ψ describes the rotation of the sample around the scattering vector $\mathbf{G}$. The $(11\bar{2})$ surface is in the scattering plane at $\psi=0$.

The present paper is organized as follows. A general expression for RXS amplitudes is obtained in Sec. II. Analysis of RXS spectra in $Ce_{1-x}La_xB_6$ are presented in Sec. III. Section IV is devoted to concluding remarks. In the Appendices, we show several expressions required to obtain the RXS amplitude formula.

II. THEORETICAL FRAMEWORK OF RXS

A. Second-order optical process

RXS is described by a second-order optical process, where a core electron is excited to unoccupied states by absorbing x rays and that electron is recombined with the core hole by emitting x rays. Since the wave function of core electron is well localized, the RXS amplitude may be given by a sum of contributions from individual ions. Using a geometrical arrangement shown in Fig. 1, we express the RXS amplitude $f(\boldsymbol{\epsilon},\boldsymbol{\epsilon}',\mathbf{k},\mathbf{k}',\omega)$ for the incident x ray with momentum $\mathbf{k}$, polarization $\boldsymbol{\epsilon}$, and the scattered x ray with momentum $\mathbf{k}'$, polarization $\boldsymbol{\epsilon}'$, as

$$f(\boldsymbol{\epsilon},\boldsymbol{\epsilon}',\mathbf{k},\mathbf{k}',\omega)=\sum_{n=1} f^{(n)}(\boldsymbol{\epsilon},\boldsymbol{\epsilon}',\mathbf{k},\mathbf{k}',\omega), \tag{2.1}$$

$$f^{(n)}(\boldsymbol{\epsilon},\boldsymbol{\epsilon}',\mathbf{k},\mathbf{k}',\omega)\propto\frac{1}{\sqrt{N}}\sum_j e^{-i\mathbf{G}\cdot\mathbf{r}_j}M_j^{(n)}(\boldsymbol{\epsilon},\boldsymbol{\epsilon}',\mathbf{k},\mathbf{k}',\omega), \tag{2.2}$$

with

$$M_j^{(1)}(\boldsymbol{\epsilon},\boldsymbol{\epsilon}',\omega)=\sum_{\mu,\mu'}\epsilon'_\mu\epsilon_{\mu'}\sum_\Lambda\frac{\langle\psi_0|x_{\mu,j}|\Lambda\rangle\langle\Lambda|x_{\mu',j}|\psi_0\rangle}{\hbar\omega-(E_\Lambda-E_0)+i\Gamma}, \tag{2.3}$$

$$M_j^{(2)}(\boldsymbol{\epsilon},\boldsymbol{\epsilon}',\mathbf{k},\mathbf{k}',\omega)=\frac{k^2}{9}\sum_{\mu,\mu'}q_\mu(\hat{\mathbf{k}}',\boldsymbol{\epsilon}')q_{\mu'}(\hat{\mathbf{k}},\boldsymbol{\epsilon})\times\sum_\Lambda\frac{\langle\psi_0|\tilde{z}_{\mu,j}|\Lambda\rangle\langle\Lambda|\tilde{z}_{\mu',j}|\psi_0\rangle}{\hbar\omega-(E_\Lambda-E_0)+i\Gamma}, \tag{2.4}$$

where $\mathbf{G}$ $(=\mathbf{k}'-\mathbf{k})$ is the scattering vector, and N is the number of sites j. The $|\psi_0\rangle$ represents the ground state with energy E_0, while $|\Lambda\rangle$ represents the intermediate state with energy E_Λ. The Γ describes the lifetime broadening width of the core hole. Equation (2.3) describes the $E1$ transition, where the dipole operators $x_{\mu,j}$ are defined as $x_{1,j}=x_j$, $x_{2,j}=y_j$, and $x_{3,j}=z_j$ in the coordinate frame fixed to the crystal axes with the origin located at the center of site j. Equation (2.4) describes the $E2$ transition, where the quadrupole operators are defined by $\tilde{z}_{1,j}=\frac{\sqrt{3}}{2}(x_j^2-y_j^2)$, $\tilde{z}_{2,j}=\frac{1}{2}(3z_j^2-r_j^2)$, $\tilde{z}_{3,j}=\sqrt{3}y_jz_j$, $\tilde{z}_{4,j}=\sqrt{3}z_jx_j$, and $\tilde{z}_{5,j}=\sqrt{3}x_jy_j$. Factors $q_\mu(\hat{\mathbf{k}},\boldsymbol{\epsilon})$ and $q_\mu(\hat{\mathbf{k}}',\boldsymbol{\epsilon}')$ with $\hat{\mathbf{k}}=\mathbf{k}/|\mathbf{k}|$ and $\hat{\mathbf{k}}'=\mathbf{k}'/|\mathbf{k}'|$ are defined as a second-rank tensor,

$$q_\mu(\mathbf{A},\mathbf{B})\equiv\begin{cases}\frac{\sqrt{3}}{2}(A_xB_x-A_yB_y) & \text{for } \mu=1,\\ \frac{1}{2}(3A_zB_z-\mathbf{A}\cdot\mathbf{B}) & \text{for } \mu=2,\\ \frac{\sqrt{3}}{2}(A_yB_z+A_zB_y) & \text{for } \mu=3,\\ \frac{\sqrt{3}}{2}(A_zB_x+A_xB_z) & \text{for } \mu=4,\\ \frac{\sqrt{3}}{2}(A_xB_y+A_yB_x) & \text{for } \mu=5.\end{cases} \tag{2.5}$$

Note that the quadrupole operators $\tilde{z}_{\mu,j}$ are expressed as $\tilde{z}_{\mu,j}=q_\mu(\mathbf{r}_j,\mathbf{r}_j)$.

B. Energy profiles

In localized electron systems, the ground state and the intermediate state are described in terms of the eigenfunctions of the angular momentum operator $|J,m\rangle$ at each site. At the ground state, the CEF and the intersite interaction usually lift the degeneracy with respect to m. We write the ground state at site j as

$$|\psi_0\rangle_j=\sum_m c_j(m)|J,m\rangle. \tag{2.6}$$

In the intermediate state, however, the CEF and the intersite interaction may be neglected in a good approximation, since their magnitudes of energy are much smaller than those of the intra-atomic Coulomb interaction and the spin-orbit interaction (SOI) which give rise to the multiplet structure. Thus the Hamiltonian describing the intermediate state is approximated as preserving the spherical symmetry. In such a circumstance, the intermediate states are characterized by the total angular momentum at the core-hole site, that is, $|\Lambda\rangle=|J',M,i\rangle$ with the magnitude J' and the magnetic quantum number M. The corresponding energy is denoted by $E_{J',i}$, where we introduce the index i in order to distinguish multiplets having the same J' value but having different energy.

In the following, we discuss only the $E2$ transition [Eq. (2.4)], because the $E1$ transition has been fully analyzed in our previous paper.[23] First, we rewrite Eq. (2.4) as

$$M_j^{(2)}(\boldsymbol{\epsilon},\boldsymbol{\epsilon}',\mathbf{k},\mathbf{k}',\omega)=\frac{k^2}{9}\sum_{\mu,\mu'}q_\mu(\hat{\mathbf{k}}',\boldsymbol{\epsilon}')q_{\mu'}(\hat{\mathbf{k}},\boldsymbol{\epsilon})M^{(2)}_{\mu\mu'}(\omega,j), \tag{2.7}$$

$$M^{(2)}_{\mu\mu'}(\omega,j)\equiv\sum_{J',M,i}E_i(\omega,J')\langle\psi_0|\tilde{z}_{\mu,j}|J',M,i\rangle\times\langle J',M,i|\tilde{z}_{\mu',j}|\psi_0\rangle, \tag{2.8}$$

with

$$E_i(\omega,J')=\frac{1}{\hbar\omega-(E_{J',i}-E_0)+i\Gamma}. \tag{2.9}$$

Then, inserting Eq. (2.6) for the ground state into Eq. (2.8), we obtain

$$M^{(2)}_{\mu\mu'}(j,\omega)=\sum_{m,m'}c_j^*(m)c_j(m')M^{(2)m,m'}_{\mu\mu'}(\omega), \tag{2.10}$$

with

$$M^{(2)m,m'}_{\mu\mu'}(\omega)=\sum_{J'}\sum_{i=1}^{N_{J'}}E_i(\omega,J')\sum_{M=-J'}^{J'}\langle J,m|\tilde{z}_\mu|J',M,i\rangle\times\langle J',M,i|\tilde{z}_{\mu'}|J,m'\rangle. \tag{2.11}$$

We have suppressed the index j specifying the core-hole site. The number of the multiplets having the value J' is denoted by $N_{J'}$. The selection rule for the $E2$ transition confines the range of the summation over J' to $J'=J$, $J\pm1$, $J\pm2$.

Now we analyze the matrix element of the type $\langle J,m|\tilde{z}_\mu|J',M\rangle$ by utilizing the Wigner-Eckart (WE) theorem for a tensor operator,[33]

$$\langle J,m|s_\mu|J'M\rangle=(-1)^{J'+m-2}\sqrt{2J+1}\begin{pmatrix}J' & 2 & J\\ M & \mu & -m\end{pmatrix}(J||V_2||J'), \tag{2.12}$$

with $s_{\pm2}=(\tilde{z}_1\pm i\tilde{z}_5)/\sqrt{2}$, $s_{\pm1}=\mp(\tilde{z}_4\pm i\tilde{z}_3)/\sqrt{2}$, and $s_0=\tilde{z}_2$. The symbol $(J||V_2||J')$ denotes the reduced matrix element of the set of irreducible tensor operator of the second rank. Because of the nature of the quadrupole operators, a condition $|m-m'|\leq4$ has to be satisfied for nonvanishing $M^{(2)m,m'}_{\mu\mu'}(\omega)$. After a straightforward but tedious calculation with the help of the WE theorem, we obtain nonzero $M^{(2)m,m'}(\omega)$'s. Then,

TABLE I. Definition of the operator equivalence of the multipole order components. The overline denotes the symmetrization, for instance, $\overline{X^2Y}=X^2Y+XYX+YX^2$.

$$z_1^{(1)}=J_x$$
$$z_2^{(1)}=J_y$$
$$z_3^{(1)}=J_z$$

$$z_1^{(2)}=O_{x^2-y^2}=\frac{\sqrt{3}}{2}[J_x^2-J_y^2]$$
$$z_2^{(2)}=O_{3z^2-r^2}=\frac{1}{2}[3J_z^2-J(J+1)]$$
$$z_3^{(2)}=O_{yz}=\frac{\sqrt{3}}{2}[J_yJ_z+J_zJ_y]$$
$$z_4^{(2)}=O_{zx}=\frac{\sqrt{3}}{2}[J_zJ_x+J_xJ_z]$$
$$z_5^{(2)}=O_{xy}=\frac{\sqrt{3}}{2}[J_xJ_y+J_yJ_x]$$

$$z_1^{(3)}=T_{xyz}=\frac{\sqrt{15}}{6}\overline{J_xJ_yJ_z}$$
$$z_2^{(3)}=T_x^{\alpha}=\frac{1}{2}[2J_x^3-\overline{J_x(J_y^2+J_z^2)}]$$
$$z_3^{(3)}=T_y^{\alpha}=\frac{1}{2}[2J_y^3-\overline{J_y(J_z^2+J_x^2)}]$$
$$z_4^{(3)}=T_z^{\alpha}=\frac{1}{2}[2J_z^3-\overline{J_z(J_x^2+J_y^2)}]$$
$$z_5^{(3)}=T_x^{\beta}=\frac{\sqrt{15}}{6}\overline{J_x(J_y^2-J_z^2)}$$
$$z_6^{(3)}=T_y^{\beta}=\frac{\sqrt{15}}{6}\overline{J_y(J_z^2-J_x^2)}$$
$$z_7^{(3)}=T_z^{\beta}=\frac{\sqrt{15}}{6}\overline{J_z(J_x^2-J_y^2)}$$

$$z_1^{(4)}=H_4^0=\frac{5}{4}\sqrt{\frac{7}{3}}\left[J_x^4+J_y^4+J_z^4-\frac{3}{5}J(J+1)\left\{J(J+1)-\frac{1}{3}\right\}\right]$$
$$z_2^{(4)}=H_4^2=-\frac{\sqrt{5}}{4}\left[\frac{7}{6}\overline{(J_x^2-J_y^2)J_z^2}-\left\{J(J+1)-\frac{5}{6}\right\}(J_x^2-J_y^2)\right]$$
$$z_3^{(4)}=H_4^4=\frac{\sqrt{5}}{48}[35J_z^4-30J(J+1)J_z^2+3J(J+1)[J(J+1)-2]+25J_z^2-7[J_x^4+J_y^4-\overline{J_x^2J_y^2}]]$$
$$z_4^{(4)}=H_x^{\alpha}=\frac{\sqrt{35}}{8}[\overline{J_x^3J_z}-\overline{J_yJ_z^3}]$$
$$z_5^{(4)}=H_y^{\alpha}=\frac{\sqrt{35}}{8}[\overline{J_z^3J_x}-\overline{J_zJ_x^3}]$$
$$z_6^{(4)}=H_z^{\alpha}=\frac{\sqrt{35}}{8}[\overline{J_x^3J_y}-\overline{J_xJ_y^3}]$$
$$z_7^{(4)}=H_x^{\beta}=\frac{\sqrt{5}}{8}[2\overline{J_x^2J_yJ_z}-(\overline{J_y^3J_z}+\overline{J_yJ_z^3})]$$
$$z_8^{(4)}=H_y^{\beta}=\frac{\sqrt{5}}{8}[2\overline{J_y^2J_zJ_x}-(\overline{J_z^3J_x}+\overline{J_zJ_x^3})]$$
$$z_9^{(4)}=H_z^{\beta}=\frac{\sqrt{5}}{8}[2\overline{J_z^2J_xJ_y}-(\overline{J_z^3J_y}+\overline{J_xJ_y^3})]$$

we perform the summation over m and m' in Eq. (2.10). The result is summarized by introducing the expectation values of the components of the multipole operators as follows:

$$M^{(2)}_{\mu,\mu'}(j,\omega)=\sum_{\nu=0}^{4}\alpha^{(\nu)}_{E2}(\omega)\sum_{\lambda=1}^{2\nu+1}[M^{(\nu)}_{\lambda}]_{\mu,\mu'}\langle\psi_0|z^{(\nu)}_{\lambda}|\psi_0\rangle, \tag{2.13}$$

where the λth component of rank ν tensor $z^{(\nu)}_{\lambda}$ in real basis $(1\le\lambda\le 2\nu+1)$ is defined in Table I. The $z^{(\nu)}_{\lambda}$ is constructed from the irreducible spherical tensor $T^{(n)}_{\lambda}$ through the unitary transformation $U^{(\nu)}$. The definitions of $T^{(\nu)}_n$ and $U^{(\nu)}$ as well as the energy profile $\alpha^{(\nu)}_{E2}(\omega)$ are given in Appendix A. The matrix element of $M^{(\nu)}_{\lambda}$ is expressed as

$$\begin{aligned}[M^{(\nu)}_{\lambda}]_{\mu,\mu'}&=\frac{(-)^{\nu}}{(2\|T_{\nu}\|2)}\sqrt{\frac{2\nu+1}{5}}\sum_{\ell=-2}^{2}\sum_{\ell'=-2}^{2}U^{(2)}_{\mu\ell}\\&\times\sum_{n=-\nu}^{\nu}U^{(\nu)}_{\lambda n}([T^{(\nu)}_n]_{\ell\ell'})^*[U^{(2)\dagger}]_{\ell'\mu'}\\&=(-)^{\nu}\sqrt{2\nu+1}\sum_{\ell=-2}^{2}\sum_{\ell'=-2}^{2}(-)^{\ell}U^{(2)}_{\mu\ell}\\&\times\sum_{n=-\nu}^{\nu}U^{(\nu)}_{\lambda n}\begin{pmatrix}2&\nu&2\\ \ell'&n&-\ell\end{pmatrix}[U^{(2)\dagger}]_{\ell'\mu'},\end{aligned} \tag{2.14}$$

with

$$(2\|T_{\nu}\|2)=\frac{1}{2^{\nu}}\sqrt{\frac{(5+\nu)!}{5(4-\nu)!}}. \tag{2.15}$$

Finally, inserting Eq. (2.13) into Eq. (2.7) and using Eq. (2.14), we obtain the final expression,

$$\begin{aligned}M^{(2)}_j(\boldsymbol{\epsilon},\boldsymbol{\epsilon}',\mathbf{k},\mathbf{k}',\omega)&=\frac{k^2}{9}\sum_{\nu=0}^{4}\alpha^{(\nu)}_{E2}(\omega)\sum_{\lambda=1}^{2\nu+1}P^{(\nu)}_{\lambda}(\boldsymbol{\epsilon},\boldsymbol{\epsilon}',\hat{\mathbf{k}},\hat{\mathbf{k}}')\\&\times\langle\psi_0|z^{(\nu)}_{\lambda}|\psi_0\rangle,\end{aligned} \tag{2.16}$$

where $P^{(\nu)}_{\lambda}$'s are the geometrical factors defined as

$$\begin{aligned}P^{(\nu)}_{\lambda}(\boldsymbol{\epsilon},\boldsymbol{\epsilon}',\hat{\mathbf{k}},\hat{\mathbf{k}}')&=\sqrt{2\nu+1}\sum_{n=-\nu}^{\nu}(-)^nU^{(\nu)}_{\lambda n}\\&\times\sum_{m=-\nu}^{\nu}\begin{pmatrix}2&2&\nu\\ m&n-m&-n\end{pmatrix}\\&\times q_m(\boldsymbol{\epsilon}',\hat{\mathbf{k}}')q_{n-m}(\boldsymbol{\epsilon},\hat{\mathbf{k}}).\end{aligned} \tag{2.17}$$

Those for $\nu=0$, 1, and 2 are expressed as relatively simple forms:

$$P^{(0)}_1(\boldsymbol{\epsilon},\boldsymbol{\epsilon}',\hat{\mathbf{k}},\hat{\mathbf{k}}')=\frac{1}{\sqrt{5}}[(\hat{\mathbf{k}}'\cdot\hat{\mathbf{k}})(\boldsymbol{\epsilon}'\cdot\boldsymbol{\epsilon})+(\hat{\mathbf{k}}'\cdot\boldsymbol{\epsilon})(\boldsymbol{\epsilon}'\cdot\hat{\mathbf{k}})], \tag{2.18}$$

$$\begin{aligned}P^{(1)}_{\mu}(\boldsymbol{\epsilon},\boldsymbol{\epsilon}',\hat{\mathbf{k}},\hat{\mathbf{k}}')&=-i\frac{1}{\sqrt{10}}[(\boldsymbol{\epsilon}'\cdot\boldsymbol{\epsilon})(\hat{\mathbf{k}}'\times\hat{\mathbf{k}})_{\mu}\\&+(\hat{\mathbf{k}}'\cdot\hat{\mathbf{k}})(\boldsymbol{\epsilon}'\times\boldsymbol{\epsilon})_{\mu}+(\mathbf{k}'\cdot\boldsymbol{\epsilon})(\boldsymbol{\epsilon}'\times\hat{\mathbf{k}})_{\mu}\\&+(\boldsymbol{\epsilon}'\cdot\hat{\mathbf{k}})(\hat{\mathbf{k}}'\times\boldsymbol{\epsilon})_{\mu},],\end{aligned} \tag{2.19}$$

$$\begin{aligned}P^{(2)}_{\mu}(\boldsymbol{\epsilon},\boldsymbol{\epsilon}',\hat{\mathbf{k}},\hat{\mathbf{k}}')&=-\frac{3}{2}\frac{1}{\sqrt{14}}[(\boldsymbol{\epsilon}'\cdot\boldsymbol{\epsilon})q_{\mu}(\hat{\mathbf{k}},\hat{\mathbf{k}}')\\&+(\hat{\mathbf{k}}'\cdot\hat{\mathbf{k}})q_{\mu}(\boldsymbol{\epsilon},\boldsymbol{\epsilon}')+q_{\mu}(\hat{\mathbf{k}}'\times\hat{\mathbf{k}},\boldsymbol{\epsilon}'\times\boldsymbol{\epsilon})].\end{aligned} \tag{2.20}$$

For $\nu=1$, indices $\mu=1$, 2, and 3 serve as the Cartesian components x, y, and z, respectively. The corresponding expres-

sion of $P_\mu^{(\nu)}$'s for $\nu=3,4$ have complicated forms, which are summarized in Appendix B.

An expression similar to Eq. (2.16) has been derived by the FCA.[15–19] However, this scheme has to put by hand the energy dependence. Therefore it is practical only to the symmetrical aspect of the azimuthal angle dependence of the RXS peak intensity when a single profile is involved. If more than two profiles belonging to the different ranks are included in a single spectrum, the interference effect among them makes it hard to get physically precise information on the azimuthal angle dependence by the FCA.

The present theory gives an explicit expression of the energy dependence, which is separated from the factor relating to the order parameter. Thus the choice of the CEF parameters in the ground state does not affect the shape of energy profiles $\alpha_{E2}^{(\nu)}(\omega)$. The applicability of our result depends on how the localized electron picture is justified in the investigated systems. Since the picture is considered reasonable in a variety of the f electron compounds, we can find lots of candidates suitable to be analyzed by the present theory. For instance, the pre-edge $E2$ signals near $L_{2,3}$ edges of CeB_6 and DyB_2C_2, the signals near $M_{2,3}$ edges of NpO_2, $U_{0.75}Np_{0.25}O_2$, and so on.

III. APPLICATION TO MULTIPOLE ORDERING PHASES IN $Ce_{1-x}La_xB_6$

In this section, we demonstrate the usefulness of Eq. (2.16) by analyzing the RXS spectra in the $E2$ transition at the Ce $L_{2,3}$ edges from $Ce_{1-x}La_xB_6$.

A. Phase II in CeB_6

The parent material CeB_6 experiences two-step phase transitions. It undergoes the first transition from paramagnetic (phase I) to an AFQ state (phase II) at $T_Q=3.2$ K and the second transition to an antiferromagnetic (AFM) state (phase III) at $T_N=2.4$ K under no external magnetic field. The AFQ order is known to be a Néel type with a propagating vector $\mathbf{Q}_0=(\frac{1}{2}\frac{1}{2}\frac{1}{2})$. On the other hand, the AFM state is double-**k** structure characterized by the modulation vectors $\mathbf{k}_1=[\frac{1}{4},\frac{1}{4},0]$ and $\mathbf{k}_2=[\frac{1}{4},-\frac{1}{4},0]$.[34,35]

These phase transitions have been theoretically studied in a localized electron scheme, where each Ce ion is assumed to be trivalent in the $4f^1$ configuration. Its ground multiplet is a Γ_8 quartet confined within the $J=\frac{5}{2}$ subspace under the cubic symmetry. Using states $\{|J_z=m\rangle\}$, the four bases $|\pm,\sigma\rangle$ ($\sigma=\uparrow,\downarrow$) may be expressed as

$$|+,\uparrow\rangle=\sqrt{\frac{5}{6}}\left|+\frac{5}{2}\right\rangle+\sqrt{\frac{1}{6}}\left|-\frac{3}{2}\right\rangle, \tag{3.1}$$

$$|-,\uparrow\rangle=\left|+\frac{1}{2}\right\rangle, \tag{3.2}$$

and $|\pm,\downarrow\rangle$ by replacing $|m\rangle$ with $|-m\rangle$. The intersite interaction may lift the fourfold degeneracy, leading to multipole orderings. Shiina *et al.* have derived such interaction from a microscopic model and obtained the phase diagram in agreement with experiments.[36,37]

Instead of pursuing this direction, we simply assume the ordering pattern, and calculate the RXS spectra. The assumed ordering pattern selects a particular energy profile according to Eq. (2.16). Note that the quartet Γ_8 consists of 16 degrees of freedom, which are exhausted by three components of dipole, five components of quadrupole, and seven components of octupole operators as well as an identical operator. Thereby the hexadecapole operators H_4^0, H_4^2, H_4^4, H_x^β, H_y^β, and H_z^β are equivalent to identical operator, $O_{x^2-y^2}$, $O_{3z^2-r^2}$, O_{yz}, O_{zx}, and O_{xy}, respectively, while $H_{x,y,z}^\alpha=0$. Therefore as long as a contribution from $\alpha_{E2}^{(2)}(\omega)$ exists, that from $\alpha_{E2}^{(4)}(\omega)$ automatically exists.

The order parameter in phase II is believed to be the O_{xy} type. Operator O_{xy} has two degenerate eigenstates of eigenvalue -1 and two degenerate eigenstates of eigenvalue $+1$, that is,

$$O_{xy}=\begin{pmatrix}-1&0&0&0\\0&-1&0&0\\0&0&1&0\\0&0&0&1\end{pmatrix}, \tag{3.3}$$

within the bases of eigenfunctions. The AFQ phase may be constructed by assigning two degenerate eigenstates with eigenvalue -1 to one sublattice and those with eigenvalue $+1$ to the other sublattice. The degeneracy of the Kramers doublet would be lifted in the AFM phase with further reducing temperatures. Within the same bases in order, typical dipole and octupole operators are represented by

$$J_z=\begin{pmatrix}-\frac{7}{6}&0&0&-\frac{2}{3}\\0&\frac{7}{6}&-\frac{2}{3}&0\\0&-\frac{2}{3}&\frac{7}{6}&0\\-\frac{2}{3}&0&0&-\frac{7}{6}\end{pmatrix}, \tag{3.4}$$

$$T_z^\beta=\begin{pmatrix}0&0&0&i3\sqrt{5}\\0&0&-i3\sqrt{5}&0\\0&i3\sqrt{5}&0&0\\-i3\sqrt{5}&0&0&0\end{pmatrix}. \tag{3.5}$$

These forms indicate that the O_{xy} order could accompany neither the J_z order nor the T_z^β order. Therefore the O_{xy} order selects the energy profiles $\alpha_{E2}^{(2)}(\omega)$ and $\alpha_{E2}^{(4)}(\omega)$ according to Eq. (2.16).

In the actual calculation of energy profile, we take into account full Coulomb interactions between $2p$ and $4f$ electrons, between $2p$ electrons, and between $4f$ electrons in the configuration $(2p)^5(4f)^2$. The spin-orbit interaction (SOI) of $2p$ and $4f$ electrons are considered too. The Slater integrals necessary for the Coulomb interactions and the SOI param-

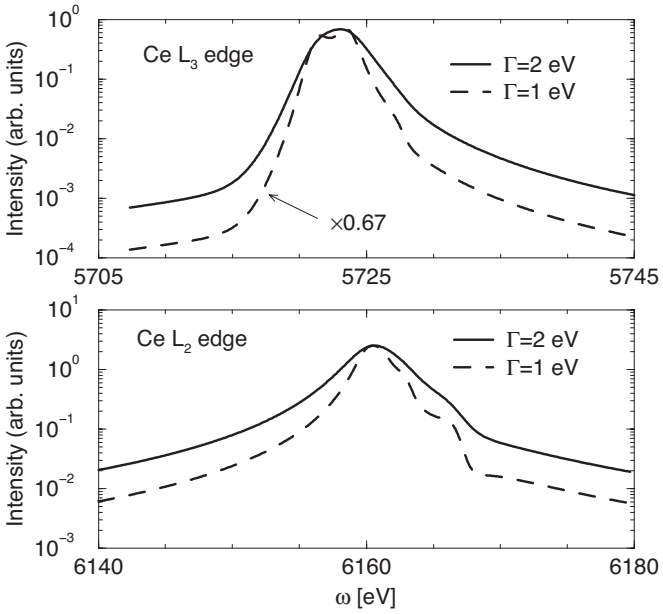

FIG. 2. The RXS spectra at the Ce L_3 (top) and L_2 (bottom) absorption edges from the AFQ phase (phase II). $\Gamma=2.0$ eV and 1.0 eV, $\mathbf{G}=(\frac{3}{2}\frac{3}{2}\frac{3}{2})$, and $\psi=0$. Three domains are assumed to have equal volumes. Only the spectra in the σ-σ' channel are displayed.

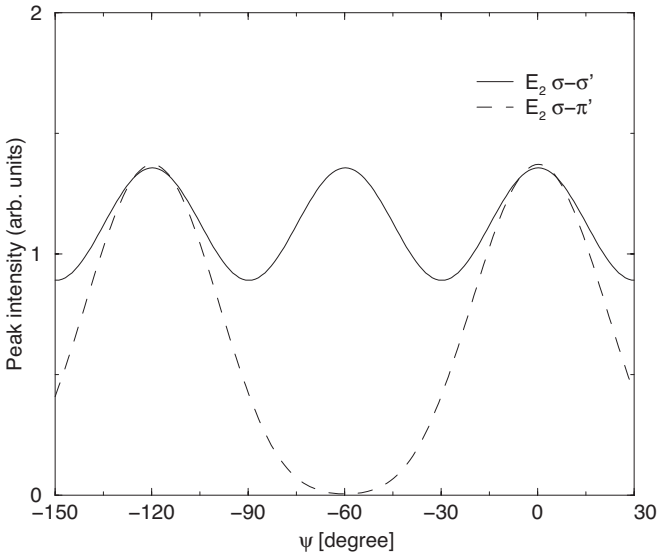

FIG. 3. The peak intensities of RXS as functions of azimuthal angle at the Ce L_3 edge from the AFQ phase (phase II). $\Gamma=2.0$ eV. Three domains are assumed to have equal volumes. The solid and broken lines represent the σ-σ' and σ-π' channels, respectively.

eters are evaluated within the Hartree-Fock approximation.[38,39]

Figure 2 shows the RXS spectra as a function of photon energy, calculated with the core-hole lifetime width $\Gamma=2.0$ and 1.0 eV. The energy of the Ce $2p$-core level is chosen such that the peak of the RXS spectra at the Ce L_3 edge coincides with the experiment for CeB_6. We find that the absolute value of $\alpha_{E2}^{(4)}(\omega)$ is much smaller than that of $\alpha_{E2}^{(2)}(\omega)$. However, the smallness is compensated by a large value of $\langle\psi_0|z_\lambda^{(4)}|\psi_0\rangle$, and thereby both terms contribute to the intensity. The calculated spectra show asymmetry and some structures, which depend on the Γ value. It may be appropriate to use $\Gamma=2.0$ eV.[40] Here, it may be helpful to compare the results obtained by our present theory with those derived by the FCA; the ratio of the maximum peak intensities of the spectra at the L_2 and L_3 edges with $\mathbf{G}=(\frac{5}{2}\frac{3}{2}\frac{3}{2})$ is found to vary around two with $\Gamma\sim 2$ eV, which is about a factor 2 smaller than that by the FCA.[30]

When the O_{xy} order is realized, the O_{yz} and O_{zx} orders are also possible to be realized. In actual crystals, three orders may constitute domains, whose structure affects the azimuthal angle dependence of the RXS spectra. Figure 3 shows the peak intensity as a function of ψ for the scattering vector $\mathbf{G}=(\frac{3}{2}\frac{3}{2}\frac{3}{2})$. The origin of ψ is defined such that the scattering plane includes the a axis. It depends strongly on domains. An incoherent addition over the contributions from three domains is performed. In the σ-σ' channel, the term of $\nu=2$ in Eq. (2.16) is independent of ψ so that the sixfold symmetry comes from the term of $\nu=4$. On the other hand, the threefold symmetry in the σ-π'channel arises from both the term of $\nu=2$ and that of $\nu=4$.

B. Phase IV in $Ce_{1-x}La_xB_6$

The La diluted material $Ce_{1-x}La_xB_6$ with $x\simeq 0.3-0.5$ has an additional phase IV whose order parameter is not well understood yet.[31] Although a large discontinuity in the specific-heat curve suggests the existence of the long-range order,[41] no neutron-scattering experiment has found an evidence of long-range magnetic order.[42,43] It is suggested[44,45] that the AFO order characterizes phase IV, which is supported by the observation of the trigonal distortion.[46] Recently, Mannix *et al.* measured the RXS spectra at the L_2 edge in the $E2$ transition in $Ce_{0.7}La_{0.3}B_6$, claiming that the signal arises from the AFO order.[27] The analysis of the azimuthal angle dependence by Kusunose and Kuramoto supports the AFO order in phase IV.[32] However, there exists at least one prominent discrepancy between the experiment and the theory about the azimuthal angle dependence which we shall address later.

Keeping two possibilities, the quadrupole and octupole orders, for phase IV, we analyze the spectra on the basis of Eq. (2.16). Since the trigonal distortion is observed along the body-diagonal direction, we assume that the order parameter is of T_{111}^β type $[T_{111}^\beta\equiv(T_x^\beta+T_y^\beta+T_z^\beta)/\sqrt{3}]$ or O_{111} type $[O_{111}\equiv(O_{xy}+O_{yz}+O_{zx})/\sqrt{3}]$. The T^α type can be ruled out because this type carries a substantial antiferromagnetic moment, which is against the experimental finding. Since $[T_{111}^\beta,O_{111}]=0$, both operators are simultaneously diagonalized. Within the bases of eigenfunctions, they are represented as

$$T_{111}^\beta=\begin{pmatrix}-3\sqrt{10} & 0 & 0 & 0\\ 0 & 3\sqrt{10} & 0 & 0\\ 0 & 0 & 0 & 0\\ 0 & 0 & 0 & 0\end{pmatrix}, \tag{3.6}$$

$$O_{111} = \begin{pmatrix} -1 & 0 & 0 & 0 \\ 0 & -1 & 0 & 0 \\ 0 & 0 & 1 & 0 \\ 0 & 0 & 0 & 1 \end{pmatrix}. \quad (3.7)$$

Within the same bases, the dipole operator J_{111} [$\equiv(J_x+J_y+J_z)/\sqrt{3}$] is represented as

$$J_{111} = \begin{pmatrix} 0 & z_1 & 0 & 0 \\ z_1^* & 0 & 0 & 0 \\ 0 & 0 & -\frac{7}{6} & 0 \\ 0 & 0 & 0 & \frac{7}{6} \end{pmatrix}, \quad (3.8)$$

where $z_1 = \frac{\sqrt{3}}{18}(1+i11\sqrt{2})$.

1. AFO order

The AFO order may be constructed by assigning the eigenstate of the T^{β}_{111} with eigenvalue $-3\sqrt{10}$ to one sublattice and that with $3\sqrt{10}$ to the other sublattice. Then, the order-parameter vector $(\langle T^{\beta}_x\rangle, \langle T^{\beta}_y\rangle, \langle T^{\beta}_z\rangle)$ is pointing to the (111) direction. Equation (3.8) indicates that the AFO order could carry no magnetic moment, which is consistent with the experiment. Equation (3.7) indicates that the AFO order accompanies the ferroquadrupole order, not the AFQ order. Therefore, according to Eq. (2.16), the RXS energy dependence is purely characterized by $|\alpha^{(3)}_{E2}(\omega)|^2$.

Figure 4 shows the calculated $|\alpha^{(3)}_{E2}(\omega)|^2$ as functions of the incident photon energy ω at the Ce L_2 and L_3 absorption edges with $\Gamma=2.0$ and 1.0 eV, in comparison with the experiment of Mannix *et al.* (the background contribution is subtracted from the data).[27] In the calculation, we use the same Slater integrals and the SOI parameters as in phase II. The spectral shapes depend strongly on the absorption edge they are observed. In particular, the tail part of the spectra at the L_3 edge is drastically different from that at the L_2 edge. This fact might be helpful to identify the character of the ordering pattern if the spectrum at the L_3 edge is experimentally available. Since the peak intensity at the L_3 edge is about 20% of that at the L_2 edge, it can be said that experimental observation has a legitimate chance at the former edge. The L_2 spectral shape reproduces well the experimental one showing broad single peak structure with a hump in the high-energy region. On the other hand, it slightly deviates from the experiment in the tail parts. Such a deviation may be remedied by choosing the better values of Γ and/or the screening multipliers. However, we do not try to get the best fitting curve to changing these parameters. This is because we notice several factors for shaking the reliability of the precision of the tail of the experimental data. First, the tail parts of the data consist of the very weak signal, about one or two orders of magnitude smaller than the peak intensity. Second, the experimental spectrum in the σ-σ' channel includes a fair amount of the background contribution, which may cause a relatively large error in the tail part of the spectrum when subtracting that contribution.

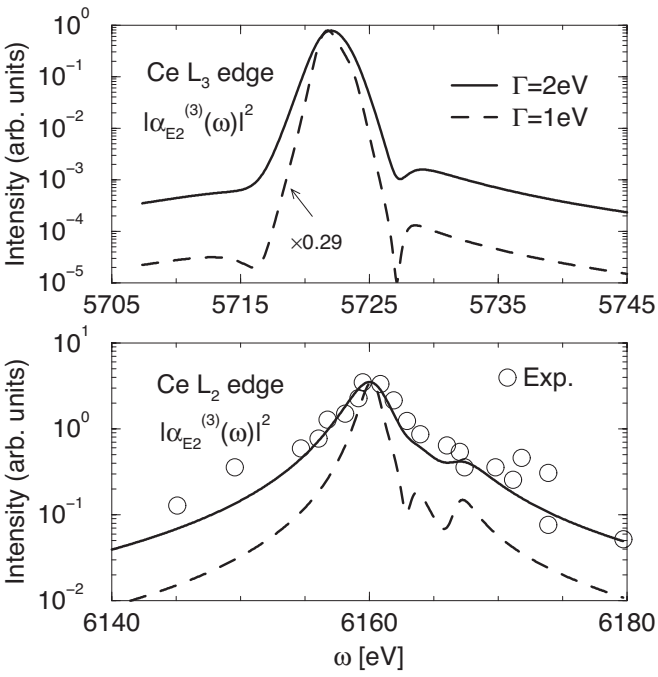

FIG. 4. Energy profile $|\alpha^{(3)}_{E2}(\omega)|^2$ at the Ce L_3 (top) and L_2 (bottom) absorption edges at $\mathbf{G}=(\frac{3}{2}\frac{3}{2}\frac{3}{2})$. Curves with $\Gamma=1.0$ eV (broken lines) are multiplied by factors 0.29 at the L_3 edge and normalized at the L_2 edge to have the same peak intensities as those with $\Gamma=2.0$ eV (solid lines). Open circles are experimental data in $Ce_{0.7}La_{0.3}B_6$, in which the background contributions are subtracted as explained by the authors (Ref. 27).

The energy profile $|\alpha^{(3)}_{E2}(\omega)|^2$ looks similar to the spectral shape in phase II (Fig. 2) for $\Gamma=2$ eV. One difference is a dip found at the L_3 edge in $|\alpha^{(3)}_{E2}(\omega)|^2$, which is absent in Fig. 2. If the Γ is as small as 1 eV, the differences are emphasized around the tail part of the high-energy region, because multiplet structures of the intermediate state are emphasized.[22] Note that, although $|\alpha^{(3)}_{E2}(\omega)|^2$ is about two orders of magnitude smaller than $|\alpha^{(2)}_{E2}(\omega)|^2$, the smallness is compensated by the large factor of $|\langle T^{\beta}_{x,y,z}\rangle|^2 \simeq 90$, resulting in the same order of magnitude of the spectral intensity as in phase II (Fig. 2).

If the octupole order-parameter vector $(\langle T^{\beta}_x\rangle, \langle T^{\beta}_y\rangle, \langle T^{\beta}_z\rangle)$ can point to the (111) direction, it is also possible to point to the $(1\bar{1}\bar{1})$, $(\bar{1}1\bar{1})$, and $(\bar{1}\bar{1}1)$ directions. These four orders usually constitute domains. The azimuthal angle dependence is different for different domains, as shown in Figs. 5(a) and 5(b). If you collect the contributions from domains with equal weight, the maximum intensity in the σ-π' channel becomes nearly equal to that in the σ-σ' channel. The experimental data show that the maximum intensity in the σ-π' channel is about half of that in the σ-σ' channel, as shown in Fig. 5(c). This may be attributed to the slightly different setup for different polarizations and/or to the extrinsic background from the nonresonant contribution, as discussed by Kusunose and Kuramoto.[32] They reduced the intensity in the σ-π' channel by simply multiplying a factor 0.6. Another possibility is that domain volumes are different among four domains. Collecting up the contributions with ratio 3:1:1:1 from the (111), $(1\bar{1}\bar{1})$, $(\bar{1}1\bar{1})$, and $(\bar{1}\bar{1}1)$ domains, we have

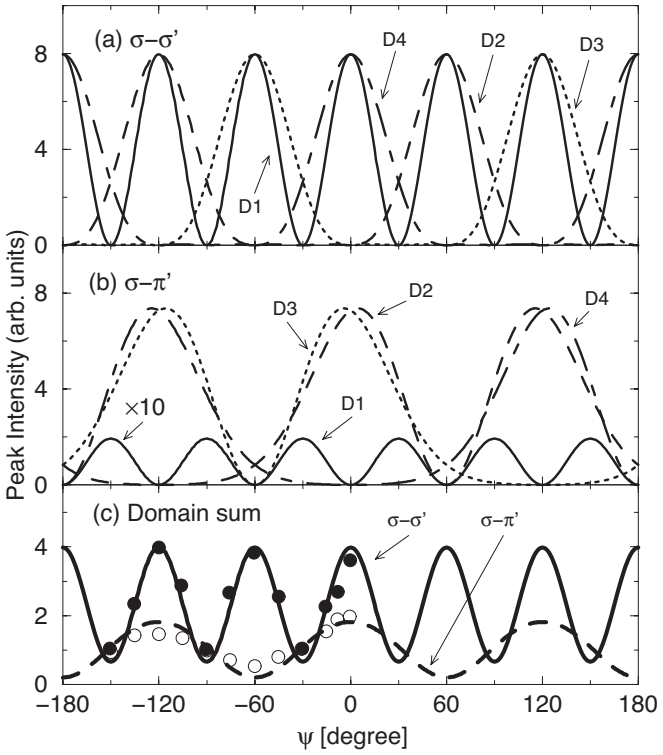

FIG. 5. Peak intensities of the RXS spectra at the Ce L_2 edges in the AFO phase as functions of the azimuthal angle. Panels (a) and (b) display the peak intensities in the σ-σ' and the σ-π' channels, respectively, where the solid (D1), broken (D2), dotted (D3), and broken-dotted (D4) lines represent the peak intensity of the domains (111), $(1\bar{1}\bar{1})$, $(\bar{1}1\bar{1})$, and $(\bar{1}\bar{1}1)$, respectively. Panel (c) shows the intensities collecting the contributions from the domains (111), $(1\bar{1}\bar{1})$, $(\bar{1}1\bar{1})$, and $(\bar{1}\bar{1}1)$ with ratio 3:1:1:1. The solid and broken lines represent the intensities in the σ-σ' and σ-π' channels, respectively. Filled and open circles are the experimental data for $Ce_{0.7}La_{0.3}B_6$ in the σ-σ' and σ-π' channels, respectively (Ref. 27).

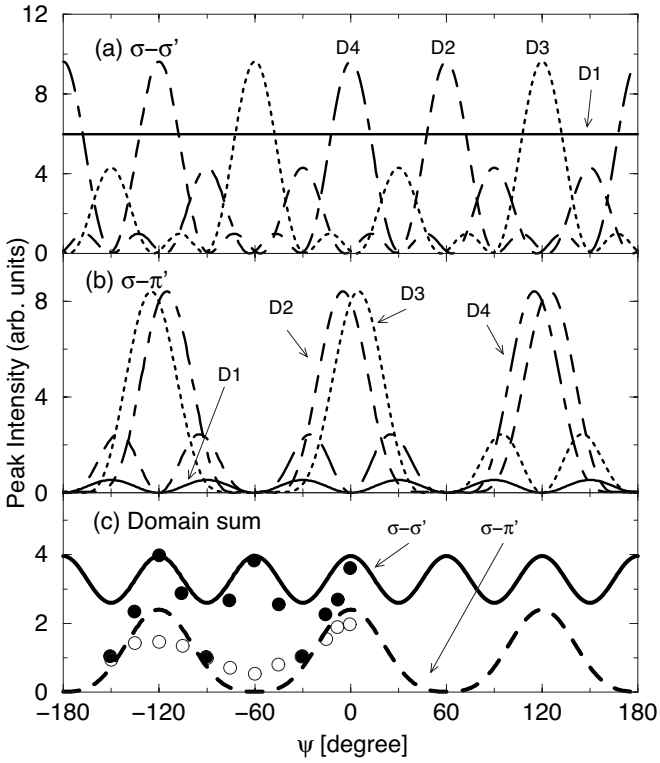

FIG. 6. Peak intensities at the Ce L_2 edges in the AFQ phase, as functions of azimuthal angle. Panels (a) and (b) display the peak intensities in the σ-σ' and the σ-π' channels, respectively, where the solid (D1), broken (D2), dotted (D3), and broken-dotted (D4) lines represent the peak intensity of the domains (111), $(1\bar{1}\bar{1})$, $(\bar{1}1\bar{1})$, and $(\bar{1}\bar{1}1)$, respectively. Panel (c) shows the result collecting the contributions from the domains with equal weight. The solid and broken lines represent the σ-σ' and σ-π' channels, respectively. The curve in the latter channel is multiplied by a factor 0.6. Filled and open circles are the experimental data for $Ce_{0.7}La_{0.3}B_6$ in the σ-σ' and σ-π' channels, respectively (Ref. 27).

the result similar to that simply multiplying a factor 0.6 to the intensity in the σ-π' channel, as shown in Fig. 5(c). Thus the sixfold and threefold symmetries in the σ-$\sigma'$and σ-π' channels are well reproduced in comparison with the experiment.

2. AFQ order

The AFQ order may be constructed by assigning the eigenstates of O_{111} with eigenvalue -1 to one sublattice and those with $+1$ to the other sublattice. The AFQ order accompanies no AFO order. The difference from phase II is that the order parameter $(\langle O_{yz}\rangle, \langle O_{zx}\rangle, \langle O_{xy}\rangle)$ is pointing to the (111) direction. Therefore the spectral shape as a function of energy is nearly the same as in phase II. The azimuthal angle dependence depends strongly on domains, which is shown in Figs. 6(a) and 6(b). The sixfold symmetry in the σ-σ' channel mainly comes not from the (111) domain but from the other domains, since the contribution from the former domain is constant with varying the azimuthal angle. Collecting the contributions from four domains with equal weight, and reducing the intensity in the σ-π' channel by multiplying a factor 0.6 in the same way as Kusunose and Kuramoto adopted,[32] we obtain the result in agreement with the experiment at least in a symmetrical point of view. Although the amplitude of the oscillation in the σ-σ'channel is too small compared with the experimental one, the situation may be changed if the subtraction of the background contribution in the σ-σ' channel and/or that of the enigmatic $E1$ contribution in the σ-π' channel are/is reevaluated. Actually, the discrepancy about the relative intensity between two channels may be attributed to the consequence of this subtraction process.

We now turn our attention to the energy dependence of the spectra. Owing to our formula Eq. (2.16), the spectral shapes from the AFQ order with O_{111} type in phase IV are the same as those with O_{xy} type in phase II (Fig. 2). Therefore the energy dependence is similar to that obtained from the AFO order at the L_2 edge, while it is different from that from the AFO order at the L_3 edge. The difference is particularly conspicuous in the higher energy part of the spectra; the spectrum from the AFQ order exhibits a rather monotonic and gradual decreasing away from the peak, while that from the AFO order shows a sharp drop of the intensity with Fano-

dip-like structure. Note that the difference is emphasized when the smaller value of $\Gamma=1$ eV is taken as shown by the broken lines in Figs. 2 and 4.

Since the symmetry consideration in the azimuthal angle dependence cannot distinguish the AFO and the AFQ orders without information on the domain distribution, spectral shape analysis of the $E2$ spectrum at the L_3 edge may help the identification of the ordering pattern realized in this material. The experimental detection is highly desired.

IV. CONCLUDING REMARKS

We have derived a general formula of the RXS amplitude in the $E2$ transition. The derivation is based on the assumption that the Hamiltonian describing the intermediate state of the scattering process preserves the spherical symmetry. The obtained formula is applicable to many f electron systems where a localized scheme gives a good description. Although similar formulas have already been obtained,[15–19] the present formula has two prominent advantages. One is that it is able to calculate the energy profile of the RXS spectra, because our treatment is free from the fast collision approximation adopted in the previous works. The other is that it is conveniently applicable to the systems possessing multipole order parameters.

We have demonstrated the usefulness of the derived formula by calculating the $E2$ RXS spectra in $Ce_{1-x}La_xB_6$. Phase II is believed to be an AFQ order of O_{xy} type, and our formula dictates that the energy dependence is given by a combination of $\alpha_{E2}^{(2)}(\omega)$ and $\alpha_{E2}^{(4)}(\omega)$. We have obtained the RXS intensity in the same order of intensity as obtained by assuming the AFO order. This suggests that the $E2$ signal is detectable from phase II, although only the $E1$ signal has been reported in phase II of CeB_6.[5,6] Subsequently, we have calculated the RXS spectra by assuming the T_{111}^{β}-type AFO order, in order to clarify the order parameter of phase IV. The energy dependence $|\alpha_{E2}^{(3)}(\omega)|^2$ has been obtained at the L_2 edge in agreement with the experiment in $Ce_{0.7}La_{0.3}B_6$.[27] Unfortunately this is not used to discriminate between the AFO and AFQ orders, because the spectral shapes are nearly the same in the two ordering phases. On the other hand, the spectral shape at the L_3 edge has been found slightly different from the L_2 edge, which might help the identification of the ordering pattern. For the azimuthal angle dependence, we have reproduced the sixfold and threefold symmetries by assuming the AFO order, in agreement with the previous theoretical analysis and the experiment.[27,32] The intensity in the σ-π' channel becomes nearly equal to that in the σ-σ' channel with the equal volume for four domains, while in the experiment the intensity in the former channel is found nearly half of that in the latter. This discrepancy may be removed by assuming uneven volumes among four domains. We have also analyzed the azimuthal angle dependence by assuming the O_{111}-type AFQ order. It is found that the simultaneously induced hexadecapole order gives rise to the sixfold and threefold symmetries. Although the agreement with the experiment is quantitatively not good, it may be difficult to rule out the AFQ order from phase IV on the basis of the azimuthal angle dependence alone. Since it depends strongly on the domain distribution, experiments controlling the domain distribution, if possible, might be useful to clarify the situation.

TABLE II. Irreducible tensor operator $T_n^{(\nu)}$ with the spherical basis.

Rank ν	n	$T_n^{(\nu)}$
1	± 1	$\mp\frac{1}{\sqrt{2}}J_{\pm}$
	0	J_z
2	± 2	$\frac{1}{2}\sqrt{\frac{3}{2}}J_{\pm}^2$
	± 1	$\mp\frac{1}{2}\sqrt{\frac{3}{2}}J_{\pm}(2J_z\pm 1)$
	0	$\frac{1}{2}[3J_z^2-J(J+1)]$
3	± 3	$\mp\frac{\sqrt{5}}{4}J_{\pm}^3$
	± 2	$\frac{\sqrt{15}}{2\sqrt{2}}J_{\pm}^2(J_z\pm 1)$
	± 1	$\mp\frac{1}{4\sqrt{3}}J_{\pm}[15J_z^2\pm 15J_z-3J(J+1)+6]$
	0	$\frac{1}{2}[5J_z^3-3J(J+1)J_z+J_z]$
4	± 4	$\frac{\sqrt{35}}{8\sqrt{2}}J_{\pm}^4$
	± 3	$\mp\frac{\sqrt{35}}{8}J_{\pm}^3(2J_z\pm 3)$
	± 2	$\frac{\sqrt{5}}{4\sqrt{2}}J_{\pm}^2[7J_z^2\pm 14J_z-J(J+1)+9]$
	± 1	$\mp\frac{\sqrt{5}}{8}J_{\pm}[14J_z^3\pm 21J_z^2+19J_z$ $-6J(J+1)J_z\mp 3J(J+1)\pm 6]$
	0	$\frac{1}{8}[35J_z^4-30J(J+1)J_z^2+25J_z^2$ $+3J^2(J+1)^2-6J(J+1)]$

ACKNOWLEDGMENTS

We thank M. Takahashi and M. Yokoyama for valuable discussions. This work was partially supported by Grants-in-Aid for Scientific Research from the Ministry of Education, Culture, Sports, Science and Technology of the Japanese Government.

APPENDIX A: DEFINITIONS OF SOME QUANTITIES USED IN SEC. II

Let us define irreducible tensor operator of rank ν with the spherical basis. The nth component $(-\nu\leq n\leq\nu)$ $T_n^{(\nu)}$ is defined recurrently as

$$T_{\nu}^{(\nu)}=(-)^{\nu}\sqrt{\frac{(2\nu-1)!!}{(2\nu)!!}}J_{+}^{\nu}, \tag{A1}$$

$$[J_{-},T_n^{(\nu)}]=\sqrt{(\nu+n)(\nu-n+1)}T_{n-1}^{(\nu)}. \tag{A2}$$

Expressions for $T_n^{(\nu)}$'s are listed in Table II up to rank 4. We can find $(2\nu+1)\times(2\nu+1)$ unitary matrix which connects the tensor operator with the spherical component $T_n^{(\nu)}$ and that with the Cartesian component $z_{\lambda}^{(\nu)}$ which satisfies

TABLE III. Unitary matrix which connects the tensor operator with the Cartesian basis and that with the spherical basis.

$$U^{(0)} = 1$$

$$U^{(1)} = \begin{pmatrix} -\frac{1}{\sqrt{2}} & 0 & \frac{1}{\sqrt{2}} \\ \frac{i}{\sqrt{2}} & 0 & \frac{i}{\sqrt{2}} \\ 0 & 1 & 0 \end{pmatrix}$$

$$U^{(2)} = \begin{pmatrix} \frac{1}{\sqrt{2}} & 0 & 0 & 0 & \frac{1}{\sqrt{2}} \\ 0 & 0 & 1 & 0 & 0 \\ 0 & \frac{i}{\sqrt{2}} & 0 & \frac{i}{\sqrt{2}} & 0 \\ 0 & -\frac{1}{\sqrt{2}} & 0 & \frac{1}{\sqrt{2}} & 0 \\ -\frac{i}{\sqrt{2}} & 0 & 0 & 0 & \frac{i}{\sqrt{2}} \end{pmatrix}$$

$$U^{(3)} = \begin{pmatrix} 0 & -\frac{i}{\sqrt{2}} & 0 & 0 & 0 & \frac{i}{\sqrt{2}} & 0 \\ -\frac{\sqrt{5}}{4} & 0 & \frac{\sqrt{3}}{4} & 0 & -\frac{\sqrt{3}}{4} & 0 & \frac{\sqrt{5}}{4} \\ -\frac{\sqrt{5}}{4}i & 0 & -\frac{\sqrt{3}}{4}i & 0 & -\frac{\sqrt{3}}{4}i & 0 & -\frac{\sqrt{5}}{4}i \\ 0 & 0 & 0 & 1 & 0 & 0 & 0 \\ \frac{\sqrt{3}}{4} & 0 & \frac{\sqrt{5}}{4} & 0 & -\frac{\sqrt{5}}{4} & 0 & -\frac{\sqrt{3}}{4} \\ -\frac{\sqrt{3}}{4}i & 0 & \frac{\sqrt{5}}{4}i & 0 & \frac{\sqrt{5}}{4}i & 0 & -\frac{\sqrt{3}}{4}i \\ 0 & \frac{1}{\sqrt{2}} & 0 & 0 & 0 & \frac{1}{\sqrt{2}} & 0 \end{pmatrix}$$

$$U^{(4)} = \begin{pmatrix} \frac{\sqrt{30}}{12} & 0 & 0 & 0 & \frac{\sqrt{21}}{6} & 0 & 0 & 0 & \frac{\sqrt{30}}{12} \\ 0 & 0 & -\frac{1}{\sqrt{2}} & 0 & 0 & 0 & -\frac{1}{\sqrt{2}} & 0 & 0 \\ -\frac{\sqrt{42}}{12} & 0 & 0 & 0 & \frac{\sqrt{15}}{6} & 0 & 0 & 0 & -\frac{\sqrt{42}}{12} \\ 0 & -\frac{i}{4} & 0 & -\frac{\sqrt{7}}{4}i & 0 & -\frac{\sqrt{7}}{4}i & 0 & -\frac{i}{4} & 0 \\ 0 & \frac{1}{4} & 0 & -\frac{\sqrt{7}}{4} & 0 & \frac{\sqrt{7}}{4} & 0 & -\frac{1}{4} & 0 \\ -\frac{i}{\sqrt{2}} & 0 & 0 & 0 & 0 & 0 & 0 & 0 & \frac{i}{\sqrt{2}} \\ 0 & \frac{\sqrt{7}}{4}i & 0 & -\frac{i}{4} & 0 & -\frac{\mathrm{i}}{4} & 0 & \frac{\sqrt{7}}{4}i & 0 \\ 0 & \frac{\sqrt{7}}{4} & 0 & \frac{1}{4} & 0 & -\frac{1}{4} & 0 & -\frac{\sqrt{7}}{4} & 0 \\ 0 & 0 & -\frac{i}{\sqrt{2}} & 0 & 0 & 0 & \frac{i}{\sqrt{2}} & 0 & 0 \end{pmatrix}$$

$$z_{\lambda}^{(\nu)} = \sum_{n=-\nu}^{\nu} U_{\lambda n}^{(\nu)} T_n^{(\nu)}, \tag{A3}$$

and inversely,

$$T_n^{(\nu)} = \sum_{\lambda=1}^{2\nu+1} [U^{(\nu)\dagger}]_{n\lambda} z_{\lambda}^{(\nu)}. \tag{A4}$$

Explicit form of $U^{(\nu)}$ is summarized in Table III.

Finally, we show the explicit forms of the functions $\alpha_{E2}^{(\nu)}(\omega)$, which give the energy profiles coupled to the expectation value of the rank-ν multipole operator,

$$\alpha_{E2}^{(4)}(\omega) = 8\sqrt{\frac{2}{35}} \sum_{J'=J-2}^{J+2} F_{J'}(\omega), \tag{A5}$$

$$\alpha_{E2}^{(3)}(\omega) = 4\sqrt{\frac{2}{5}}[-(2J-3)F_{J-2} - (J-2)F_{J-1} + 2F_J + (J+3)F_{J+1} + (2J+5)F_{J+2}], \tag{A6}$$

$$\alpha_{E2}^{(2)}(\omega) = 2\sqrt{\frac{2}{7}}\left[4(2J-3)(J-1)F_{J-2} + (J-5)(J-1)F_{J-1} - \frac{1}{3}(2J-3)(2J+5)F_J + (J+2)(J+6)F_{J+1} + 4(2J+5)(J+2)F_{J+2}\right], \tag{A7}$$

$$\alpha_{E2}^{(1)}(\omega) \equiv -\sqrt{\frac{2}{5}}[4(J-1)(2J-1)(2J-3)F_{J-2} - (J-1) \times (2J-1)(J+3)F_{J-1} + (2J-1)(2J+3)F_J + (J+2)(J-2)(2J+3)F_{J+1} - 4(J+2)(2J+3) \times (2J+5)F_{J+2}], \quad \text{(A8)}$$

$$\alpha_{E2}^{(0)}(\omega) \equiv \frac{2}{3\sqrt{5}}[6J(J-1)(2J-1)(2J-3)F_{J-2} - 3J(J-1)(J+1)(2J-1)F_{J-1} + J(J+1)(2J-1)(2J+3)F_J - 3J(J+1)(J+2)(2J+3)F_{J+1} + 6(J+1)(J+2)(2J+3)(2J+5)F_{J+2}]. \quad \text{(A9)}$$

The energy dependence is contained in the functions $F_{J'}(\omega)$ as

$$F_{J'}(\omega) = {}_4\mathrm{C}_{J-J'+2}\sqrt{(2J+1)(2J'+1)}\frac{(J+J'-2)!}{(J+J'+3)!} \times |(J\|V_2\|J')|^2 \sum_{i=1}^{N_{J'}} E_i(\omega, J'), \quad \text{(A10)}$$

where ${}_n\mathrm{C}_m = \frac{n!}{m!(n-m)!}$ represents the combination.

APPENDIX B: GEOMETRICAL FACTORS

The geometrical factors $P_\mu^{(\nu)}$ for $\nu=3$ and 4 in Eq. (2.16) have rather complicated forms. For $\nu=3$, they are summarized as follows:

$$P_1^{(3)} \equiv i\frac{1}{3\sqrt{2}}\{[\hat{\mathbf{k}}' \times \hat{\mathbf{k}}] \cdot \mathbf{q}(\boldsymbol{\epsilon}', \boldsymbol{\epsilon}) + [\boldsymbol{\epsilon}' \times \boldsymbol{\epsilon}] \cdot \mathbf{q}(\hat{\mathbf{k}}', \hat{\mathbf{k}}) + [\hat{\mathbf{k}}' \times \boldsymbol{\epsilon}] \cdot \mathbf{q}(\boldsymbol{\epsilon}', \hat{\mathbf{k}}) + [\boldsymbol{\epsilon}' \times \hat{\mathbf{k}}] \cdot \mathbf{q}(\hat{\mathbf{k}}', \boldsymbol{\epsilon})\}, \quad \text{(B1)}$$

$$P_\mu^{(3)} = \frac{i}{2}\sqrt{\frac{5}{2}}\{[\hat{\mathbf{k}}' \times \hat{\mathbf{k}}]_\mu \epsilon'_\mu \epsilon_\mu + [\boldsymbol{\epsilon}' \times \boldsymbol{\epsilon}]_\mu \hat{k}'_\mu \hat{k}_\mu + [\hat{\mathbf{k}}' \times \boldsymbol{\epsilon}]_\mu \epsilon'_\mu \hat{k}_\mu + [\boldsymbol{\epsilon}' \times \hat{\mathbf{k}}]_\mu \hat{k}'_\mu \epsilon_\mu\} + \frac{i}{2\sqrt{10}}P_\mu^{(1)}$$

for $\mu = 2$, 3, and 4, (B2)

$$P_\mu^{(3)} = \frac{i}{4}\sqrt{\frac{3}{2}}(\hat{\mathbf{k}}' \times \hat{\mathbf{k}})_\mu \sum_{\mu',\mu''=5}^{7} \epsilon_{\mu\mu'\mu''}(\epsilon'_{\mu'}\epsilon_{\mu'} - \epsilon'_{\mu''}\epsilon_{\mu''}) + \frac{i}{4}\sqrt{\frac{3}{2}}(\boldsymbol{\epsilon}' \times \boldsymbol{\epsilon})_\mu \sum_{\mu',\mu''=5}^{7} \epsilon_{\mu\mu'\mu''}(\hat{k}'_{\mu'}\hat{k}_{\mu'} - \hat{k}'_{\mu''}\hat{k}_{\mu''}) + \frac{i}{4}\sqrt{\frac{3}{2}}(\hat{\mathbf{k}}' \times \boldsymbol{\epsilon})_\mu \sum_{\mu',\mu''=5}^{7} \epsilon_{\mu\mu'\mu''}(\epsilon'_{\mu'}\hat{k}_{\mu'} - \epsilon'_{\mu''}\hat{k}_{\mu''}) + \frac{i}{4}\sqrt{\frac{3}{2}}(\boldsymbol{\epsilon}' \times \hat{\mathbf{k}})_\mu \sum_{\mu',\mu''=5}^{7} \epsilon_{\mu\mu'\mu''}(\hat{k}'_{\mu'}\epsilon_{\mu'} - \hat{k}'_{\mu''}\epsilon_{\mu''})$$

for $\mu = 5$, 6, and 7. (B3)

Note that $\mu=2$, 3, and 4 work as x, y, and z, respectively. Similarly, $\mu=5$, 6, and 7 work as x, y, and z, respectively. The Levi-Civita tensor density $\epsilon_{\mu\mu'\mu''}$ is introduced.

For $\nu=4$, the results are as follows:

$$P_1^{(4)} = \sqrt{\frac{2}{15}}[5(\hat{k}'_x\hat{k}_x\epsilon'_x\epsilon_x + \hat{k}'_y\hat{k}_y\epsilon'_y\epsilon_y + \hat{k}'_z\hat{k}_z\epsilon'_z\epsilon_z) - P_1^{(0)}], \quad \text{(B4)}$$

$$P_2^{(4)} = \sqrt{14}(\hat{k}'_x\hat{k}_x\epsilon'_x\epsilon_x - \hat{k}'_y\hat{k}_y\epsilon'_y\epsilon_y) - 2\sqrt{\frac{2}{21}}\{[\hat{\mathbf{k}}' \cdot \hat{\mathbf{k}}]q_1(\boldsymbol{\epsilon}', \boldsymbol{\epsilon}) + [\boldsymbol{\epsilon}' \cdot \boldsymbol{\epsilon}]q_1(\hat{\mathbf{k}}', \hat{\mathbf{k}}) + [\hat{\mathbf{k}}' \cdot \boldsymbol{\epsilon}]q_1(\boldsymbol{\epsilon}', \hat{\mathbf{k}}) + [\boldsymbol{\epsilon}' \cdot \hat{\mathbf{k}}]q_1(\hat{\mathbf{k}}', \boldsymbol{\epsilon})\}, \quad \text{(B5)}$$

$$P_3^{(4)} = -\sqrt{14}[\hat{k}'_x\hat{k}_x\epsilon'_x\epsilon_x + \hat{k}'_y\hat{k}_y\epsilon'_y\epsilon_y - 2\hat{k}'_z\hat{k}_z\epsilon'_z\epsilon_z] - 2\sqrt{\frac{2}{7}}\{[\hat{\mathbf{k}}' \cdot \hat{\mathbf{k}}]q_2(\boldsymbol{\epsilon}', \boldsymbol{\epsilon}) + [\boldsymbol{\epsilon}' \cdot \boldsymbol{\epsilon}]q_2(\hat{\mathbf{k}}', \hat{\mathbf{k}}) + [\hat{\mathbf{k}}' \cdot \boldsymbol{\epsilon}]q_2(\boldsymbol{\epsilon}', \hat{\mathbf{k}}) + [\boldsymbol{\epsilon}' \cdot \hat{\mathbf{k}}]q_2(\hat{\mathbf{k}}', \boldsymbol{\epsilon})\}, \quad \text{(B6)}$$

$$P_\mu^{(4)} = \frac{1}{2\sqrt{6}}q_{\mu+1}(\hat{\mathbf{k}}', \hat{\mathbf{k}}) \sum_{\mu',\mu''=4}^{6} \epsilon_{\mu\mu'\mu''}(\epsilon'_{\mu'}\epsilon_{\mu'} - \epsilon'_{\mu''}\epsilon_{\mu''}) + \frac{1}{2\sqrt{6}}q_{\mu+1}(\boldsymbol{\epsilon}', \boldsymbol{\epsilon}) \sum_{\mu',\mu''=4}^{6} \epsilon_{\mu\mu'\mu''}(\hat{k}'_{\mu'}\hat{k}_{\mu'} - \hat{k}'_{\mu''}\hat{k}_{\mu''}) + \frac{1}{2\sqrt{6}}q_{\mu+1}(\hat{\mathbf{k}}', \boldsymbol{\epsilon}) \sum_{\mu',\mu''=4}^{6} \epsilon_{\mu\mu'\mu''}(\epsilon'_{\mu'}\hat{k}_{\mu'} - \epsilon'_{\mu''}\hat{k}_{\mu''}) + \frac{1}{2\sqrt{6}}q_{\mu+1}(\boldsymbol{\epsilon}', \hat{\mathbf{k}}) \sum_{\mu',\mu''=4}^{6} \epsilon_{\mu\mu'\mu''}(\hat{k}'_{\mu'}\epsilon_{\mu'} - \hat{k}'_{\mu''}\epsilon_{\mu''})$$

for $\mu = 4$, 5, and 6, (B7)

$$P_\mu^{(4)} = \frac{1}{\sqrt{42}}[7\hat{k}'_\mu\hat{k}_\mu - 3(\hat{\mathbf{k}}' \cdot \hat{\mathbf{k}})]q_{\mu-4}(\boldsymbol{\epsilon}', \boldsymbol{\epsilon}) + \frac{1}{\sqrt{42}}[7\epsilon'_\mu\epsilon_\mu - 3(\boldsymbol{\epsilon}' \cdot \boldsymbol{\epsilon})]q_{\mu-4}(\hat{\mathbf{k}}', \hat{\mathbf{k}}) + \frac{1}{\sqrt{42}}[7\epsilon'_\mu\hat{k}_\mu - 3(\boldsymbol{\epsilon}' \cdot \hat{\mathbf{k}})]q_{\mu-4}(\hat{\mathbf{k}}', \boldsymbol{\epsilon}) + \frac{1}{\sqrt{42}}[7\hat{k}'_\mu\epsilon_\mu - 3(\hat{\mathbf{k}}' \cdot \boldsymbol{\epsilon})]q_{\mu-4}(\boldsymbol{\epsilon}', \hat{\mathbf{k}})$$

for $\mu = 7$, 8, and 9, (B8)

where indices 4, 5, and 6 in the summations in Eq. (B7) serve as x, y, and z, respectively. Similarly, indices 7, 8, and 9 appearing in the brackets in Eq. (B8) serve as x, y, and z, respectively.

[1] Y. Murakami, H. Kawada, H. Kawata, M. Tanaka, T. Arima, Y. Moritomo, and Y. Tokura, Phys. Rev. Lett. **80**, 1932 (1998).
[2] Y. Murakami, J. P. Hill, D. Gibbs, M. Blume, I. Koyama, M. Tanaka, H. Kawata, T. Arima, Y. Tokura, K. Hirota, and Y. Endoh, Phys. Rev. Lett. **81**, 582 (1998).
[3] H. Ohsumi, Y. Murakami, T. Kiyama, H. Nakao, M. Kubota, Y. Wakabayashi, Y. Konishi, M. Izumi, M. Kawasaki, and Y. Tokura, J. Phys. Soc. Jpn. **72**, 1006 (2003).
[4] J. Igarashi and M. Takahashi, Phys. Scr. **72**, CC1 (2005), and references therein.
[5] H. Nakao, K. Magishi, Y. Wakabayashi, Y. Murakami, K. Koyama, K. Hirota, Y. Endoh, and S. Kunii, J. Phys. Soc. Jpn. **70**, 1857 (2001).
[6] F. Yakhou, V. Plakhty, H. Suzuki, S. Gavrilov, P. Burlet, L. Paolasini, C. Vettier, and S. Kunii, Phys. Lett. A **285**, 191 (2001).
[7] K. Hirota, N. Oumi, T. Matsumura, H. Nakao, Y. Wakabayashi, Y. Murakami, and Y. Endoh, Phys. Rev. Lett. **84**, 2706 (2000).
[8] Y. Tanaka, T. Inami, T. Nakamura, H. Yamauchi, H. Onodera, K. Ohoyama, and Y. Yamaguchi, J. Phys.: Condens. Matter **11**, L505 (1999).
[9] T. Nagao and J. Igarashi, J. Phys. Soc. Jpn. **70**, 2892 (2001).
[10] J. Igarashi and T. Nagao, J. Phys. Soc. Jpn. **71**, 1771 (2002).
[11] G. T. Trammel, Phys. Rev. **126**, 1045 (1962).
[12] F. de Bergevin and M. Brunel, Acta Crystallogr., Sect. A: Cryst. Phys., Diffr., Theor. Gen. Crystallogr. **37**, 314 (1981).
[13] S. W. Lovesey, J. Phys. C **20**, 5625 (1987).
[14] M. Blume and D. Gibbs, Phys. Rev. B **37**, 1779 (1988).
[15] J. P. Hannon, G. T. Trammell, M. Blume, and D. Gibbs, Phys. Rev. Lett. **61**, 1245 (1988); **62**, 2644 (1989).
[16] J. Luo, G. T. Trammell, and J. P. Hannon, Phys. Rev. Lett. **71**, 287 (1993).
[17] P. Carra and B. T. Thole, Rev. Mod. Phys. **66**, 1509 (1994).
[18] S. W. Lovesey and E. Balcar, J. Phys.: Condens. Matter **8**, 10983 (1996).
[19] J. P. Hill and D. F. McMorrow, Acta Crystallogr., Sect. A: Found. Crystallogr. **52**, 236 (1996).
[20] J. A. Paixão, C. Detlefs, M. J. Longfield, R. Caciuffo, P. Santini, N. Bernhoeft, J. Rebizant, and G. H. Lander, Phys. Rev. Lett. **89**, 187202 (2002).
[21] S. B. Wilkins, J. A. Paixão, R. Caciuffo, P. Javorsky, F. Wastin, J. Rebizant, C. Detlefs, N. Bernhoeft, P. Santini, and G. H. Lander, Phys. Rev. B **70**, 214402 (2004).
[22] T. Nagao and J. Igarashi, J. Phys. Soc. Jpn. **74**, 765 (2005).
[23] T. Nagao and J. Igarashi, Phys. Rev. B **72**, 174421 (2005).
[24] T. Nagao and J. Igarashi, J. Phys. Soc. Jpn. **75**, Suppl. 247 (2006).
[25] E. D. Isaacs, D. B. McWhan, R. N. Kleiman, D. J. Bishop, G. E. Ice, P. Zschack, B. D. Gaulin, T. E. Mason, J. D. Garrett, and W. J. L. Buyers, Phys. Rev. Lett. **65**, 3185 (1990).
[26] N. Bernhoeft, G. H. Lander, M. J. Longfield, S. Langridge, D. Mannix, E. Lidström, E. Colineau, A. Hiess, C. Vettier, F. Wastin, J. Rebizant, and P. Lejay, Acta Phys. Pol. B **34**, 1367 (2003).
[27] D. Mannix, Y. Tanaka, D. Carbone, N. Bernhoeft, and S. Kunii, Phys. Rev. Lett. **95**, 117206 (2005).
[28] S. B. Wilkins, R. Caciuffo, C. Detlefs, J. Rebizant, E. Colineau, F. Wastin, and G. H. Lander, Phys. Rev. B **73**, 060406(R) (2006).
[29] P. Blum and F. Bertaut, Acta Crystallogr. **7**, 81 (1954).
[30] S. W. Lovesey, J. Phys.: Condens. Matter **14**, 4415 (2002).
[31] T. Tayama, T. Sakakibara, K. Tenya, H. Amitsuka, and S. Kunii, J. Phys. Soc. Jpn. **66**, 2268 (1997).
[32] H. Kusunose and Y. Kuramoto, J. Phys. Soc. Jpn. **74**, 3139 (2005).
[33] A. Messiah, *Quantum Mechanics* (North-Holland, Amsterdam, 1962).
[34] J. M. Effantin, J. Rossat-Mignod, P. Burlet, H. Bartholin, S. Kunii, and T. Kasuya, J. Magn. Magn. Mater. **47-48**, 145 (1985).
[35] O. Zaharko, P. Fischer, A. Schenck, S. Kunii, P. J. Brown, F. Tasset, and T. Hansen, Phys. Rev. B **68**, 214401 (2003).
[36] R. Shiina, H. Shiba, and P. Thalmeier, J. Phys. Soc. Jpn. **66**, 1741 (1997).
[37] H. Shiba, O. Sakai, and R. Shiina, J. Phys. Soc. Jpn. **68**, 1988 (1999).
[38] R. Cowan, *The Theory of Atomic Structure and Spectra* (University of California Press, Berkeley, 1981).
[39] In solids, the magnitude of the Slater integrals are known to be reduced due to a large screening effect. The isotropic and the anisotropic parts of the Slater integral are used by multiplying factors 0.25 and 0.8, respectively.
[40] M. H. Chen, B. Crasemann, and H. Mark, Phys. Rev. A **24**, 177 (1981).
[41] T. Furuno, N. Sato, S. Kunii, T. Kasuya, and W. Sasaki, J. Phys. Soc. Jpn. **54**, 1899 (1985).
[42] H. Takigawa, K. Ohishi, J. Akimitsu, W. Higemoto, and R. Kadono, J. Phys. Soc. Jpn. **71**, 31 (2002).
[43] P. Fischer, K. Iwasa, K. Kuwahara, M. Kohgi, T. Hansen, and S. Kunii, Phys. Rev. B **72**, 014414 (2005).
[44] K. Kubo and Y. Kuramoto, J. Phys. Soc. Jpn. **72**, 1859 (2003).
[45] K. Kubo and Y. Kuramoto, J. Phys. Soc. Jpn. **73**, 216 (2004).
[46] M. Akatsu, T. Goto, Y. Nemoto, O. Suzuki, S. Nakamura, and S. Kunii, J. Phys. Soc. Jpn. **72**, 205 (2003).